674–683 *Nucleic Acids Research, 2022, Vol. 50, No. 2* *Published online 8 January 2022*
https://doi.org/10.1093/nar/gkab1277

Metallohelix vectors for efficient gene delivery via cationic DNA nanoparticles

Jaroslav Malina[1], Hana Kostrhunova[1], Vojtech Novohradsky[1], Peter Scott[2] and Viktor Brabec[1,*]

[1]Czech Academy of Sciences, Institute of Biophysics, Brno, CZ-61265, Czech Republic and [2]Department of Chemistry, University of Warwick, Coventry, CV4 7AL, UK

Received November 04, 2021; Revised December 07, 2021; Editorial Decision December 08, 2021; Accepted December 14, 2021

ABSTRACT

The design of efficient and safe gene delivery vehicles remains a major challenge for the application of gene therapy. Of the many reported gene delivery systems, metal complexes with high affinity for nucleic acids are emerging as an attractive option. We have discovered that certain metallohelices—optically pure, self-assembling triple-stranded arrays of fully encapsulated Fe—act as nonviral DNA delivery vectors capable of mediating efficient gene transfection. They induce formation of globular DNA particles which protect the DNA from degradation by various restriction endonucleases, are of suitable size and electrostatic potential for efficient membrane transport and are successfully processed by cells. The activity is highly structure-dependent—compact and shorter metallohelix enantiomers are far less efficient than less compact and longer enantiomers.

GRAPHICAL ABSTRACT

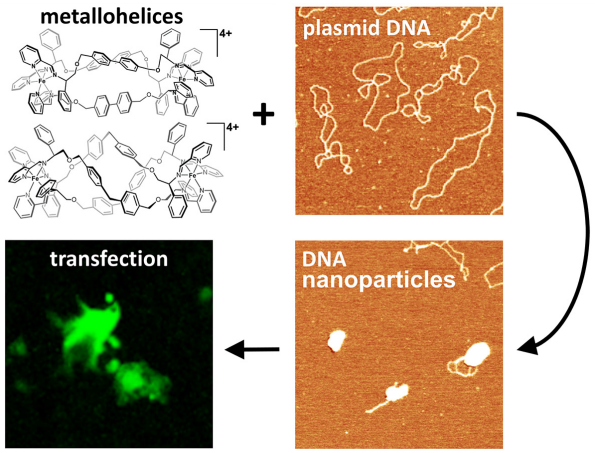

INTRODUCTION

Over the past 30 years, gene therapy, which is based on the delivery of genetic material to the cells (1,2), has made significant progress as a potential interventions for genetic disorders (3,4) or cancer (5), which are difficult to treat with traditional approaches. The design of efficient and safe gene delivery vehicles remains a major challenge for the application of this therapy (6) since free nucleic acids are rapidly degraded by nucleases present in the blood and the repulsive electrostatic interactions between DNA/RNA and the cell membrane, both negatively charged, can limit uptake into cells. Generally, two types of gene delivery vectors are used: viral agents and a broad array of synthetic systems (7) [polyamines (8), polycations (9), polymers (10), polypeptides (11), lipids (12), cyclodextrin (13) and dendrimers (14)]. Viral vectors, despite being highly effective, suffer from major drawbacks such as limited cargo capacity, resistance to repeated infections, difficulty in production and quality control, and low safety due to the toxic and immune response they induce (15,16). Synthetic chemical carriers have a number of advantages over viral vectors, such as improved safety, lack of immunogenicity, high gene loading capacity and simple preparation (17).

Of the many reported gene delivery systems, metal complexes with high affinity to nucleic acids are emerging as an attractive option for developing nonviral gene delivery vectors. As potential DNA condensing agents, metal complexes offer several advantages. They exhibit a high positive charge density (usually 2+ or higher) required for the neutralization of the negatively charged DNA backbone, which is essential for DNA condensation to occur. Ligands in coordination complexes can be functionalized for specific targeting, cellular uptake or accumulation. Moreover, some metal centers can exhibit spectroscopic properties that can be exploited for luminescent tracking of intracellular gene expression.

There are many metal complexes with high positive charges that have been studied for DNA condensing activity (18). However, few have been tested in gene delivery. Ru complexes are among the most popular, and their

*To whom correspondence should be addressed. Tel: +420 541517148; Email: brabec@ibp.cz

luminescent properties are often used for direct tracking of the DNA condensates (19–23). Other metal complexes that have been studied for their potential as DNA carriers were mainly based on Co(II) (24–27), Cu(II) (28), Ca(II) (26) but also on La(III) (29).

The condensed DNA nanoparticles are believed to enter the cells via membrane endocytosis. This process is facilitated by the positive zeta potential of the nanoparticles, which enhances their association with the negatively charged cellular membrane. The effectivity of the cellular uptake was shown to be also dependent on the size of the DNA condensates. DNA nanoparticles induced by dinuclear Co(II) and Ca(II) complexes having 50–150 nm in diameter were taken up more than those with diameters of <30 nm or >200 nm (28). Upon entering the cytoplasm, the DNA condensates must reach the nucleus to get access to the transcriptional machinery. Metal complexes as gene carriers may offer protection for DNA from degradation in the cytoplasm, and in the ideal case, they should also help with the transport of DNA to the nucleus. The transfection efficacy of DNA condensates can be promoted by the application of positively charged peptides, such as cell-penetrating peptides (CPPs) (30) and nuclear localization sequences (NLSs) (27).

We previously reported that supramolecular triple-stranded helicates $[Fe_2L_3]Cl_4$ ($L = C_{25}H_{20}N_4$) are efficient DNA condensers that induce the formation of globular DNA particles (~60 nm in diameter) and protect DNA against degradation by various restriction endonucleases (31). Our investigations of DNA interactions of two $[Co_2L_3]^{6+}$ cylinders derived from bis(bidentate) 2-pyridyl-1,2,3-triazole ligands revealed that both cylinders effectively condensed/aggregated DNA and were even able to induce condensation of chromatin in living cells (32). Recently we have studied the biological activity, and DNA binding properties of a series of highly water-stable, self-assembling optically pure Fe(II) metallohelices and obtained results showed that some metallohelices exhibited a high affinity to DNA and were able to condense DNA molecules more efficiently than conventional condensing agents such as polyamines (33). Such metallohelices were also capable of inhibiting DNA-related enzymatic activities such as DNA transcription, DNA relaxation by topoisomerase I and DNA cleavage by the EcoRI restriction endonuclease. These properties are all structure-dependent; metallohelices or various structures in a number of different architectures are available in both enantiomeric forms via versatile and rational routes (34–38).

These findings encouraged us to investigate the potency of three selected enantiomeric pairs of Fe(II) metallohelices (Figure 1) as nonviral DNA delivery vectors. The choice of bridging aromatic units allows us to assess the effect of helix length and fold.

MATERIALS AND METHODS

Chemicals

The Fe(II) metallohelices $[Fe_2\mathbf{L}^n{}_3]Cl_4$ were synthesized as previously described (34,37). The stock solutions were prepared in water at the concentration of 1–2 mM. All of the common chemicals and reagents were obtained from Merck and were used as received.

Total intensity light scattering

A 1.5 μM solution of plasmid gWiz-Luc (6732 bp; Aldevron, Fargo, ND, USA) was prepared in 10 mM cacodylate buffer (pH 7.2) in a total volume of 2.5 ml. Small volumes (<10 μl) of metallohelices were added to the DNA solution in a 1 cm quartz cuvette to obtain the desired concentration. The mixture was thoroughly mixed by pipetting and left undisturbed for 3 min at RT. Total intensity light scattering was measured at 90° angle with respect to the incident beam by using Varian Cary Eclipse spectrofluorophotometer with the following parameters: the excitation and emission wavelengths were set to 305 nm, the excitation and emission slit widths were 5 nm, and the averaging time was set to 3 s.

Gel retardation assay

Plasmid DNA gWiz-Luc (20 ng μl^{-1}) was treated with various concentrations of metallohelices in 10 mM Tris-HCl buffer (pH 7.4) in a total volume of 10 μl. After 15 min incubation at RT, 1.2 μl of loading dye (0.25% bromophenol blue, 60% glycerol) was added to the mixtures, and the samples were separated by electrophoresis on 0.9% native agarose gel running at 25 ^{o}C with 1 × TAE (Tris-acetate/EDTA) buffer for 150 min and the voltage set at 40 V. The gels were stained with GelRed (Biotium, CA, USA), followed by photography with transilluminator.

Reversibility of DNA condensation

Plasmid gWiz-Luc (6.25×10^{-5} M, per nucleotide) was first treated with metallohelices (4.2×10^{-5} M) in 10 mM Tris-HCl buffer (pH 7.4) and incubated for 15 min at RT. Then increasing concentrations of NaCl, KCl or $MgCl_2$ were added to the mixtures and samples were left for 30 min at RT. Finally, the samples were analyzed by electrophoresis at the same conditions as the method mentioned previously.

AFM imaging

Metallohelices were mixed with 20 ng of plasmid gWiz-Luc in 4 mM HEPES buffer (pH 7.4) with 5 mM KCl and 5 mM $MgCl_2$ in a total volume of 10 μl and incubated at room temperature for 10 min. The mixture was spotted in a 4 μl volume on freshly cleaved mica (SPI, West Chester, PA) and left to incubate for 2 min. Then, the mica surface was gently rinsed with 0.5 ml of Milli-Q water and immediately blown dry with compressed air. AFM images were collected in the air using a Bruker MultiMode 8 instrument operated in ScanAsyst-HR mode with SCANASYST-AIR-HR probes (Bruker, Santa Barbara, CA).

Displacement of Hoechst 33258 (H33258) and methyl green (MG)

A mixture of 1×10^{-5} M CT DNA and 1×10^{-6} M H33258 or MG was prepared in Tris-HCl buffer (pH 7.4) in the absence or the presence of 50 mM NaCl in a total volume

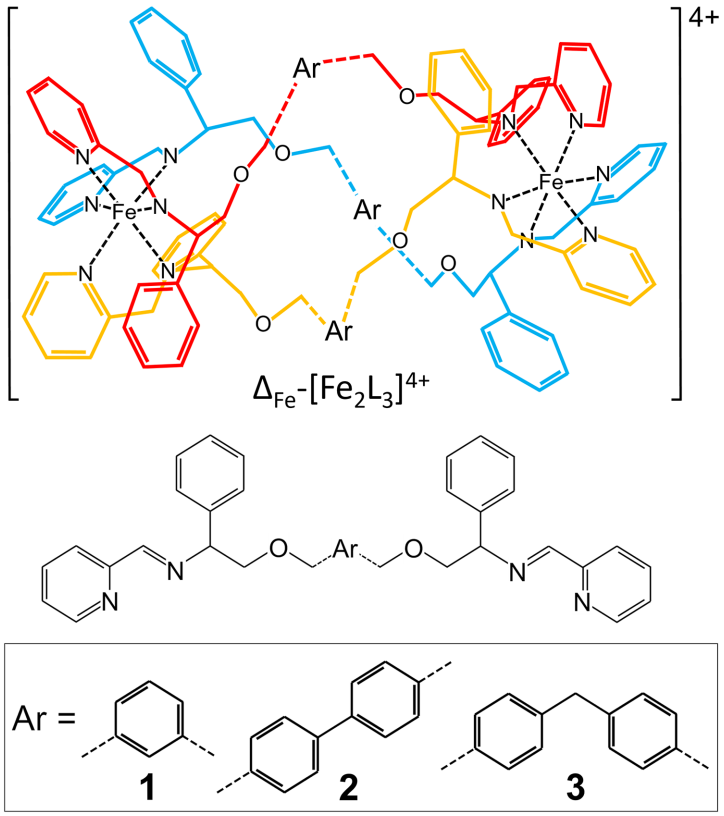

Figure 1. Structures of the investigated Fe(II) metallohelices. Both Λ_{Fe} and Δ_{Fe} enantiomers were prepared for each metallohelix.

of 0.6 ml. Small amounts of metallohelices were added to the solution in a 0.5 × 0.5 cm quartz cuvette to obtain the desired concentration and thoroughly mixed by pipetting. The mixture was left undisturbed for 3 min at RT. The fluorescence of H33258 or MG was then measured by using the Varian Cary Eclipse spectrofluorophotometer. Excitation and emission wavelengths were set to 338 and 452 nm for H33258 and 633 and 677 nm for MG, respectively. A decrease in the fluorescence intensity was plotted against the concentration of metallohelices, and the concentration of the metallohelix causing a half-maximal effect (DC_{50}) was determined.

Size and zeta potential measurement

Plasmid gWiz-Luc (1.75×10^{-5} M, per nucleotide) was mixed with metallohelices (1.17×10^{-5} M) in 10 mM Tris-HCl buffer (pH 7.4) and incubated for 10 min at RT in a total volume of 100 μl. Samples were then 10 times diluted with 10 mM Tris-HCl buffer (pH 7.4) to the final volume of 1 ml. Both apparent hydrodynamic diameters and zeta potentials of the DNA condensates were determined by using Zetasizer Ultra (Malvern, UK) at 25 ºC. Data were analyzed within the built-in ZS Xplorer software.

Nanoparticle tracking analysis (NTA)

Samples were prepared in the same way as for size and zeta potential measurements and analyzed by NanoSight NS300 (Malvern, UK) equipped with the 488 nm blue laser module and syringe pump. For each measurement, 2 min video was recorded with the cell temperature set to 25 ºC and syringe speed set to 40 μl s^{-1}. Captured videos were analyzed by the supplied NanoSight Software NTA 3.1 with a detection threshold of 5.

Cellular uptake

HEK 293 cells were seeded in 8-chamber microslides (ibidi) at a density of 10^4 cells/well and incubated overnight in a complete DMEM medium. gWiz-GFP plasmid DNA (10 μM) was incubated with individual metallohelices at DNA base:metallohelix ratio 1:0.8 at 37 °C for 15 min in Opti-MEM® medium (Gibco). GelRed™ Nucleic Acid Stain (Biotium, 10 000×) was then added. Following another 10 min incubation (RT), the DMEM medium was removed from the microslide chambers and replaced with Opti-MEM medium containing preincubated DNA samples. The incubation at 37°C proceeded for 120 min. The cells were then fixed with p-formaldehyde (4% in PBS) and mounted with ProLong Diamond Antifade Mountant with DAPI (Invitrogen). The imaging was performed with laser-scanning microscope Leica TCS SP8 SMD (Leica Microsystems, GmbH, Wetzlar, Germany).

Cell viability

HEK 293 cells were grown and treated as stated below for GFP imaging (4 h with condensates and additional 72 h in DMEM) except that gWiz-blank DNA (no transgene)

was used instead of gWiz-GFP. DNA concentration was 12.5 μM and DNA base:metallohelix ratio was 1:0.2; 1:0.4; 1:0.8; 1:1.2 and 1:1.6. At the end of the experiment, the cells were trypsinized and resuspended in DMEM. Aliquots of the suspension were combined with Trypan Blue Dye (0.4% solution, 1:1, BIO-RAD) and analyzed with Automated Cell Counter (TC10™, BIO-RAD).

GFP imaging

HEK 293 cells were seeded on glass coverslips in 6-well plates and grown overnight in DMEM. DNA condensates were prepared as follows: DNA (gWiz-GFP plasmid; Aldevron, USA) was incubated (RT) with metallohelices (DNA 2 μg ml^{-1}; DNA base:metallohelix ratio 1:1.2) in Opti-MEM® medium (Gibco) for 15 min. DMEM was removed from the wells and replaced with metallohelix-induced DNA condensate samples. Following a 4 h incubation at 37 °C (humidified atmosphere, 5% CO_2), the Opti-MEM medium was withdrawn, and the cells were incubated for another 72 h in DMEM. The cells were then fixed with 4% p-formaldehyde, washed with PBS, and mounted with ProLong™ Diamond Antifade. The imaging was performed with laser-scanning microscope Leica TCS SP8 SMD (Leica Microsystems, GmbH, Wetzlar, Germany)

Flow cytometry

HEK 293 cells were grown and incubated with metallohelix-DNA condensates in 6-well plates. The metallohelix-induced DNA condensates were prepared as above. Three or four DNA base:metallohelix ratios were analyzed. To account for fluorescence interference of the helicates, samples containing Blank plasmid DNA (gWiz-blank plasmid, no transgene, Aldevron, USA) were also analyzed. Following a 4 h incubation with the DNA condensates and consequent 72 h incubation in compound-free DMEM, the cells were harvested and fixed with 4% p-formaldehyde. The cells were then analyzed with FACS Verse flow cytometer (Becton Dickinson, Germany), and the obtained data were analyzed with FCS Express Flow Cytometry Software 6 (De Novo Software).

RESULTS AND DISCUSSION

First, we investigated the ability of metallohelices to condense DNA since this is a prerequisite for the transport of gene vectors in cells.

Total intensity light scattering

A total intensity light scattering study was performed to explore the DNA condensation transition induced by metallohelices. This method is based on measuring the intensity of the light scattered by the condensed DNA particles upon the addition of metallohelix to the diluted solution of plasmid DNA using a right-angle configuration. The plots in Figure 2 demonstrate that **2** and **3** are far more efficient inducers of DNA condensation than **1** and that the DNA condensates formed with **2** and **3** are of similar size. The midpoints of DNA condensation for **Λ-3** and **Δ-3**

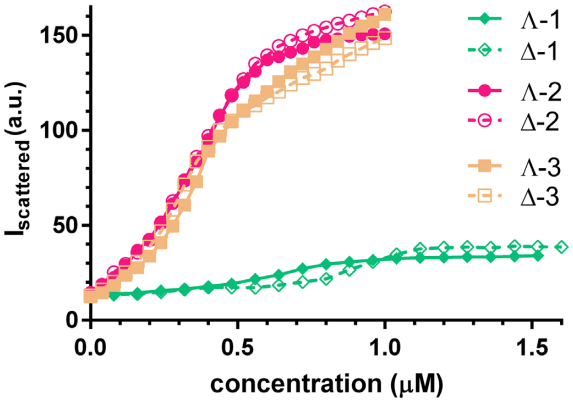

Figure 2. Light scattering of gWiz-Luc plasmid DNA solution in the presence of increasing concentrations of metallohelices. The concentration of DNA was 1.5 μM (per nucleotide), and the buffer conditions were 10 mM sodium cacodylate (pH 7.2).

were at ∼0.30 and ∼0.32 μM concentrations, respectively, while both enantiomers of **2** were slightly less active with the transition midpoint at ∼0.38 μM concentration. These concentrations ranging from 0.30 to 0.38 μM correspond to the ∼5–4:1 (DNA base:metallohelix) ratio, respectively, and comply with the requirement that ∼90% of the negative charges of DNA phosphates must be neutralized before the DNA condensation can occur (39). The less active Λ- and Δ-enantiomers of **1** had their transition midpoints at higher concentrations of ∼0.6 and ∼0.9 μM, respectively. The lower scattering produced by DNA condensates promoted by **1** indicates that these particles differ from those promoted by **2** and **3**.

Gel retardation assay

The DNA condensing ability of metallohelices was further confirmed by gel retardation assay. The results in Figure 3 show that all metallohelices reduce the amount of free DNA in the gel and that when the concentration of metallohelices reached 42, 28 and 19 μM for **1**, **2** and **3**, respectively, most of the DNA remained in the loading wells. The differences between **2** and **3** and between their enantiomers were small; however, **3** appeared to be a slightly more efficient condensing agent than **2,** which is in agreement with the results of light scattering experiments (Figure 2). Both enantiomers of **1** were at the highest concentrations able to condense most of the plasmid DNA. Still, the presence of DNA smearing (upper panel in Figure 3) indicates that the condensed DNA molecules are slowly released from the wells during electrophoresis. DNA decondensation could be caused by the effect of an electric field or electrophoresis buffer (Tris-acetate-EDTA) or by a combination of both.

Reversibility of DNA condensation

It is known that DNA condensation by multivalent cations can be reversed by the addition of monovalent (Na^+, K^+) and divalent (Mg^{2+}, Zn^{2+}, Ca^{2+}) cations, which compete with multivalent cations for the negatively charged phosphates in the DNA sugar-phosphate backbone (40,41).

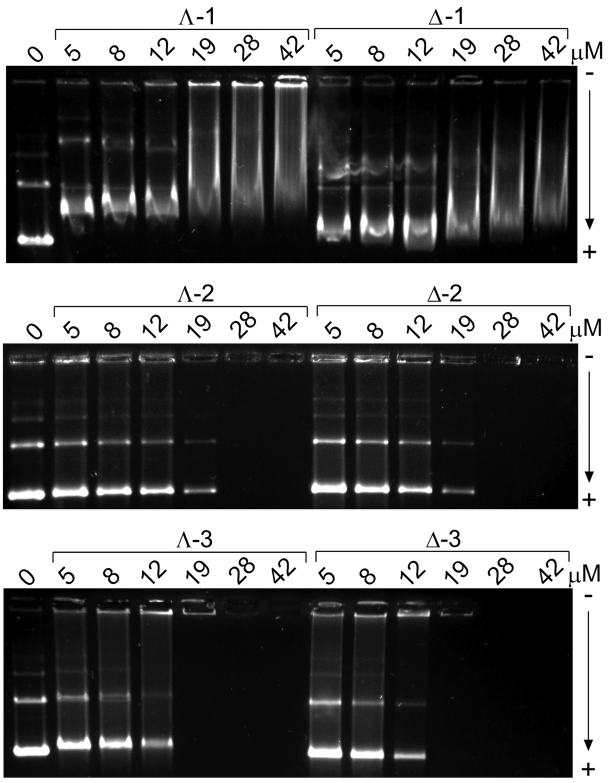

Figure 3. Effect of **1**, **2** and **3** on the migration of plasmid gWiz-Luc (6732 bp) in the native 0.9% agarose gel. The DNA and metallohelices were incubated prior to electrophoresis for 15 min in 10 mM Tris-HCl buffer (pH 7.4). The DNA concentration in the samples was 62.5 μM and the concentrations of metallohelices are indicated in the Figure.

DNA condensates of **1**, **2** and **3** were treated with increasing concentrations of NaCl, KCl and $MgCl_2$ to examine the ability of these endogenous cationic species to reverse DNA condensation. The samples were left to equilibrate for 30 min, and the DNA decondensation was visualized by the reappearance of the band for plasmid DNA. Gels in Supplementary Figures S1–S3 show that applying high concentrations of Na^+, K^+ and Mg^{2+} did not lead to the release of DNA molecules from DNA condensates formed by **2** and **3**. Conversely, the reappearance of the band for plasmid DNA was observed for DNA condensed by **1** at the concentrations of Na^+, K^+ and Mg^{2+} as low as 100, 50 and 6 mM, respectively. It is in agreement with our previous report showing that the binding of **1** to double-stranded (ds) DNA was more weakened by the increased ionic strength than the binding of **2** and **3** (42). It suggests that the binding of **1** to ds DNA is more dependent on the electrostatic interactions.

Atomic force microscopy (AFM) imaging

DNA condensation by metallohelices and the morphology of the resulting condensates were monitored by AFM. Samples were deposited onto freshly cleaved mica and imaged after drying in the air. A typical image of uncondensed gWiz-Luc plasmids is provided for comparison in Supplementary Figure S4. Supplementary Figure S5 shows representative images of plasmid gWiz-Luc in the presence of increasing concentrations of **Λ-1** and **Δ-1**. As can be seen in Supplementary Figure S5A and D, both enantiomers of **1** had to be applied at 6.24 μM concentration (1:1, DNA base:metallohelix ratio) to induce the formation of DNA particles (typically, ∼50–150 nm in diameter), but most of the plasmid molecules were still free and just loosely associated. Doubling the concentration of metallohelices to 12.5 μM (Supplementary Figure S5B,E) resulted in the reduction of the fraction of free DNA molecules, and a slightly higher condensing activity of the Λ-enantiomer was more apparent. When the concentration was finally raised to 25 μM (1:4, DNA base:metallohelix ratio), the difference between both enantiomers was obvious (Supplementary Figure S5C,F). While **Λ-1** promoted the formation of large clusters of densely packed DNA aggregates, images of plasmid DNA in the presence of **Δ-1** still contained many free DNA molecules. The higher potency of **Λ-1** to condense DNA is consistent with the previous experiments. Representative images of DNA molecules condensed by **2** and **3** are presented in Supplementary Figures S6 and S7, respectively. In both cases, concentrations as low as 1.04 and 0.78 μM for **2** and **3**, respectively, were sufficient to observe large clusters of DNA aggregates and the absence of free plasmid molecules. Panels A and D in Supplementary Figures S6 and S7 show that much smaller concentrations, 0.52 μM for **2** and 0.39 μM for **3**, of both metallohelices lead to the formation of DNA particles that were slightly larger (∼100–200 nm in diameter) than those formed by **1**. A slight increase of the concentrations of **2** and **3** to 0.78 and 0.52 μM, respectively (panels B and E in Supplementary Figure S6 and S7) resulted in the reduction of free DNA molecules and the occasional appearance of larger DNA aggregates. Overall, AFM imaging confirmed that metallohelices **2** and **3** are potent condensers of DNA and that **3** is a slightly better condensing agent than **2**. The low condensing activity of **1** in this assay can be attributed to the composition of the buffer for AFM imaging which contains K^+ and Mg^{2+} cations necessary for DNA adsorption on a mica surface shown in the gel retardation assay experiments above to weaken the interaction of **1** with ds DNA. The reduced occurrence of DNA condensates of **1** in the AFM images could also result from the drying of the samples deposited on mica with compressed air, which can disrupt weakly condensed and aggregated DNA molecules (43).

DNA displacement assays

The lower DNA condensing activity of **1** might be caused by its lower binding affinity to ds DNA or by a different binding mode compared to **2** and **3**. The apparent binding constant (K_{app}) of **1** determined by the displacement of an intercalating dye ethidium bromide from ds DNA was, however, slightly higher than K_{app}s determined for **2** and **3** (33). To gain additional information about the binding of **1**, **2** and **3,** we carried out DNA displacement assays with two other dyes, Hoechst 33258 (H33258) and methyl green (MG). Bisbenzimide H33258 is a fluorescent DNA stain that binds strongly in the minor groove of ds DNA,(44) whereas MG dye binds in the major groove of ds DNA (45). Mixtures of calf thymus (CT) DNA with H33258 or MG were prepared in 10 mM Tris-HCl (pH 7.4) in the absence and the presence

Table 1. DC_{50} values (μM) for CT DNA determined by the displacement of Hoechst 33258 (H33258) and methyl green (MG) upon addition of the metallohelices in 10 mM Tris-HCl (pH 7.4) in the absence and the presence of 50 mM NaCl.

	H33258 (DC_{50})		MG (DC_{50})	
Compound	no NaCl	50 mM NaCl	no NaCl	50 mM NaCl
Λ-1	0.24 ± 0.04	2.7 ± 0.2	0.91 ± 0.07	5.9 ± 0.4
Δ-1	0.51 ± 0.03	7.2 ± 0.4	1.66 ± 0.06	17.6 ± 0.8
Λ-2	0.76 ± 0.04	0.95 ± 0.08	1.75 ± 0.08	1.85 ± 0.04
Δ-2	0.81 ± 0.04	0.93 ± 0.06	1.44 ± 0.04	1.66 ± 0.09
Λ-3	0.54 ± 0.02	0.72 ± 0.04	1.21 ± 0.05	1.31 ± 0.06
Δ-3	0.60 ± 0.05	0.89 ± 0.03	1.36 ± 0.07	1.51 ± 0.05

Table 2. Size, zeta potential, and concentration of the plasmid gWiz-Luc condensates induced by metallohelices at 1.5:1 (DNA base:metallohelix) ratio in 10 mM Tris-HCl buffer (pH 7.4) obtained with the aid of Zetasizer Ultra and NanoSight NS300 instruments.

	Zetasizer		NanoSight		
Compound	Size (nm)	Zeta potential (mV)	Size (nm)	Concentration (10^9 particle/ml)	No of valid tracks
Λ-1	1092 ± 67	-23 ± 3	n/a	n/a	204
Δ-1	1104 ± 140	-26 ± 3	n/a	n/a	330
Λ-2	114 ± 13	41 ± 4	138 ± 39	1.68	11192
Δ-2	94 ± 15	39 ± 5	127 ± 36	1.67	11421
Λ-3	114 ± 8	30 ± 4	139 ± 41	1.42	9675
Δ-3	92 ± 10	36 ± 4	119 ± 39	1.28	9252

of 50 mM NaCl and titrated with metallohelices. The efficacy of **1**, **2** and **3** to displace both dyes was quantified by determining the DC_{50} value, which is the concentration of a metallohelix at a 50% reduction of dye fluorescence. The data in Table 1 show that at low salt conditions **Λ-1** and **Δ-1**, with the DC_{50} values of 0.24 and 0.51 μM, respectively, were very efficient at displacing H33258 from ds DNA and that **Λ-1** was even the best displacer of H33258. However, the presence of 50 mM NaCl dramatically weakened the binding of **Λ-1** and **Δ-1** to ds DNA and the DC_{50} values of both enantiomers were elevated >10-fold whereas the DC_{50} values of **2** and **3** was increased by <50%. The displacement of MG by **1**–**3** gave similar results. The binding affinities of both enantiomers of **1** were higher or comparable to those of **2** and **3** and **Λ-1** was again identified as the most potent binder with the DC_{50} value of 0.91 μM. The DC_{50} values of **Δ-1** and the enantiomers of **2** and **3** were a little higher between 1.21 and 1.75 μM. The addition of 50 mM NaCl lead to a dramatic increase of the DC_{50} values of **Λ-1** and **Δ-1** by ∼6- and ∼10-fold, respectively, while the DC_{50} values of **2** and **3** were raised by <20%. Taken together, the results of DNA displacement assays do not indicate a different binding mode for **1** compared to **2** and **3** and show that in low salt conditions, **Λ-1** and **Δ-1** bind to ds DNA with high affinity. In accord with the previous results, the binding of **1** to ds DNA was confirmed to be strongly dependent on the ionic strength, which is consistent with the idea that the binding of **1** to double-helical DNA is more dependent on the electrostatic interactions. The results also suggest that the slightly higher condensing activity of **3** compared to **2** could be attributed to its slightly higher binding affinity to ds DNA.

Size and zeta potential measurements

The apparent hydrodynamic diameters of DNA condensates induced by **1**, **2** and **3** were evaluated by DLS measurements. The plasmid gWiz-Luc was mixed with metallohelices at a 1.5:1 (DNA base:metallohelix) ratio in 10 mM Tris-HCl buffer (pH 7.4). Data in Table 2 reveal that while the diameters of the DNA condensates formed with **2** and **3** fluctuated between 92 and 114 nm, **Λ-1** and **Δ-1** promoted the formation of 10-fold larger DNA particles. In order to verify the results from DLS, we employed the nanoparticle tracking analysis (NTA) technique under the same experimental conditions. The sizes of DNA particles induced by **2** and **3** were close to the data from DLS in the range of 119–139 nm (see Table 2 and Supplementary Figures S13–S16) and in good agreement with AFM imaging (Supplementary Figures S5–S7). The concentrations of DNA particles promoted by **2** and **3** were comparable between 1.28 and 1.68 × 10^9 particle/ml. The attempts to measure the size and concentration of DNA condensates formed with **1** by NTA were, however, not successful. The numbers of valid particle tracks obtained for DNA condensates of **1** were by order of magnitude lower than those of **2** and **3** (Table 2) and did not allow proper statistical analysis (Supplementary Figures S11 and S12). The captured videos of plasmid DNA mixed with **1** contained apparently smaller amounts of particles than the videos of plasmid DNA in the presence of **2** and **3,** but at the same time, they also contained highly scattering large objects resembling clusters of smaller particles (compare still images from videos in Supplementary Figures S8–S10). The build-in software was unable to track the movement of these particles, probably because the size of these objects was beyond the detection limit of the NTA instrument (∼1000 nm).

Finally, zeta potentials of the DNA condensates were determined by the Zetasizer instrument. The DNA particles promoted by **2** and **3** had quite high positive zeta potentials between 29.7 and 40.9 mV that are equal or higher than the commonly accepted limit of ±30 mV for a stable system and should promote good stability of the particles and limit their tendency to aggregate (46). Since most cellular membranes are negatively charged, the positive zeta potential can affect the ability of nanoparticles to perme-

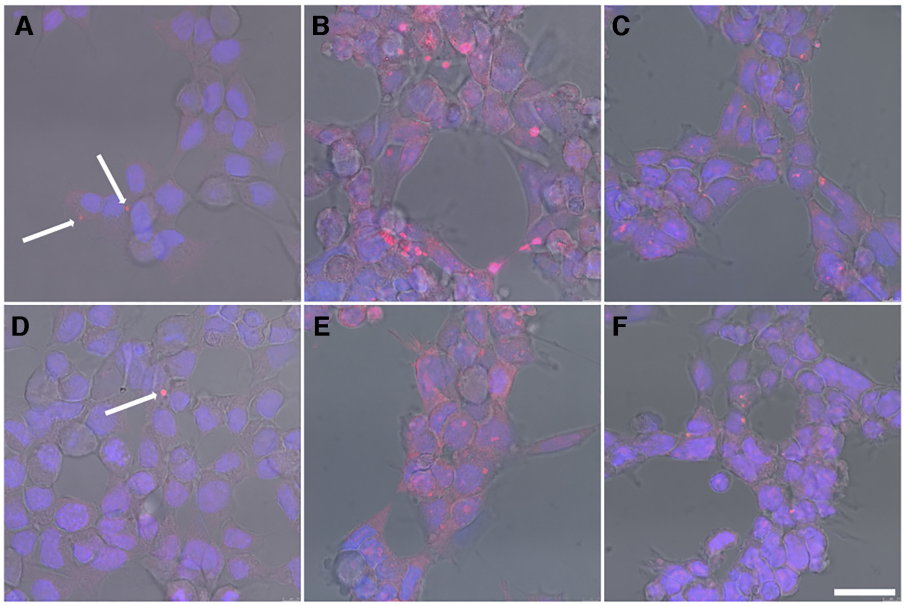

Figure 4. Monitoring of cellular uptake of DNA condensates. Plasmid gWiz-GFP was incubated with individual metallohelices at 1:0.8 DNA base:metallohelix ratio for 15 min. The DNA was then stained with GelRed and incubated with HEK 293 cells for 120 min. The cells were counter-stained with DAPI. (**A**) **Λ-1**, (**D**) **Δ-1**, (**B**) **Λ-2**, (**E**) **Δ-2**, (**C**) **Λ-3** and (**F**) **Δ-3**; scale bar: 25 μm.

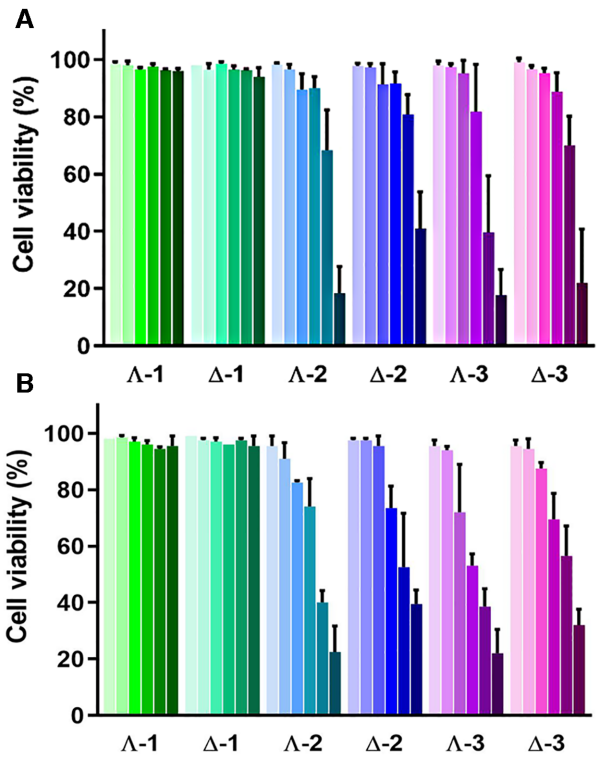

Figure 5. Cell viabilities determined with trypan blue following the treatment of HEK 293 cells with DNA condensates (**A**) or metallohelices alone (**B**). (A) The cells were treated with DNA condensates for 4 h and grew in a drug-free medium for another 72 h. DNA concentration was 12.5 μM and DNA base:metallohelix ratios were 1:0.1; 1:0.2; 1:0.4; 1:0.8; 1:1.2 and 1:1.6. (B) The cells were treated with the metallohelices alone for 4 h and grew in drug-free medium for another 72 h. The concentrations of the metallohelices were identical to those used in the cell viability experiment with DNA condensates (A), i.e. 1.25, 2.5, 5, 10, 15 and 20 μM. Each data point represents the mean of three independent experiments.

ate membranes. On the contrary, DNA condensates formed with **Λ-1** and **Δ-1** were anionic with zeta potentials of -22.8 and -26.3 mV, respectively. This was unexpected since the measurements of zeta potential were conducted at low salt conditions in which **1** exhibits high binding affinity toward ds DNA. Therefore, the lower absolute values of the zeta potential make the DNA particles promoted by **1** less stable and more prone to aggregation.

Cellular uptake

Following the DNA condensation, entering the condensates into cells is the first step necessary for efficient transfection. The presence of pre-stained DNA within HEK 293 cells was directly observed using confocal microscopy (Figure 4). As can be seen, red spots corresponding to the metallohelix-induced DNA condensates were recognized in all samples, although the internalization of DNA condensates promoted by **Λ-1** and **Δ-1** was rare (see arrows in Figure 4A,D). Conversely, multitudinous red fluorescent spots confirming successful cellular uptake were observed for DNA condensates formed with **Λ-3**, **Δ-3** (Figure 4C,F) and particularly for those formed with **Λ-2** and **Δ-2** (Figure 4B,E).

Cell viability

Cytotoxicity is a critical factor for the successful application of a synthetic gene delivery vector, and therefore we evaluated the viability of cells after the transfection with DNA condensates prepared at various DNA base:metallohelix ratios. Results in Figure 5A reveal that no apparent reduction in viability of cells treated with DNA condensates of **1** was observed under the conditions used. Cells incubated with DNA condensates of the remaining metallohelices retained

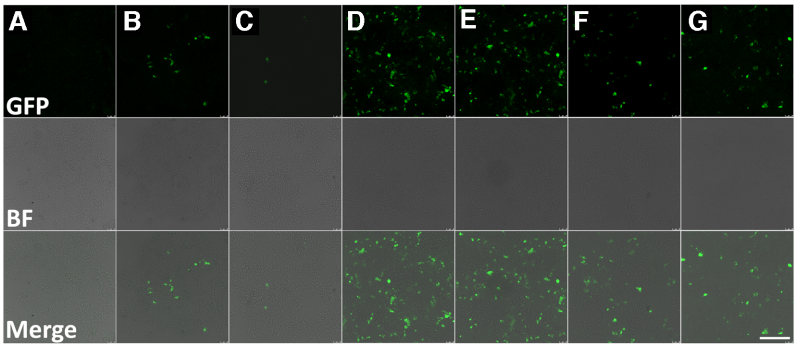

Figure 6. GFP fluorescence in HEK 293 cells. The cells were incubated with DNA condensates (1:1.2, DNA base:metallohelix) for 4 h and then grew in the compound-free medium for 72 h. The cells were fixed with 4% p-formaldehyde and mounted with ProLong™ Diamond Antifade. GFP, Green fluorescence protein; BF, Bright field; Merge. (**A**) control; (**B**) **Λ-1**; (**C**) **Δ-1**; (**D**) **Λ-2**; (**E**) **Δ-2**; (**F**) **Λ-3**; (**G**) **Δ-3**; scale bar: 200 μm.

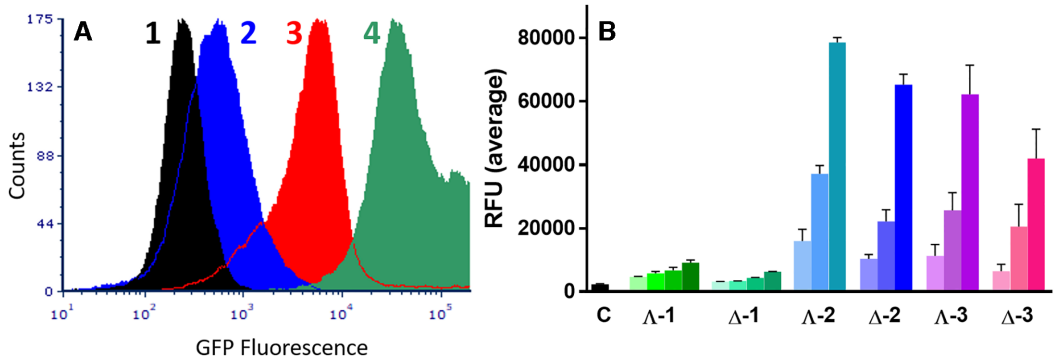

Figure 7. Flow cytometry analysis of GFP fluorescence in HEK 293 cells treated with DNA condensates induced by metallohelices. The cells were incubated with DNA condensates prepared at various DNA base:metallohelix ratios for 4 h in Opti-MEM. The medium was then replaced with DMEM, and the cells were incubated for another 72 h, harvested, and fixed with 4% p-formaldehyde. The samples were analyzed with FACS Verse flow cytometer, and data were analyzed with FCS Express flow cytometry software 6. (**A**) Representative fluorescence profiles; 1, control (no metallohelix), 2, cells treated with blank-DNA condensates of **Λ-2** (1:1.2 molar ratio), 3, cells treated with GFP-DNA condensates of **Λ-2** (1:1.2 molar ratio); 4, cells treated with GFP-DNA condensates of Lipofectamine. (**B**) Quantitative analysis of GFP fluorescence profiles. C – control cells containing only GFP-DNA; **Λ-2** and **Δ-2** were mixed with DNA at DNA base:metallohelix ratios of 1:0.4, 1:0.8; 1:1.2 and 1:1.6; **Λ-2**, **Δ-2**, **Λ-3** and **Δ-3** were mixed with DNA at DNA base:metallohelix ratios of 1:0.4, 1:0.8 and 1:1.2. Each data point represents the mean of three independent experiments.

viability above 80% up to the DNA base:metallohelix ratio of 1:0.8 and in the case of **Δ-2** even up to the ratio of 1:1.2. However, the use of DNA condensates formed with higher concentrations of **2** and **3** metallohelices reduced cell viability to levels below 50%. Generally, the DNA condensates formed by the Δ-enantiomers of **2** and **3** were slightly less toxic than those formed by the Λ-enantiomers. Interestingly, the results in Figure 5B show that the investigated metallohelices alone affected the viability of HEK 293 cells approximately to the same extent as the metallohelices in their DNA condensates. Moreover, no correlation has been observed between the cell viability of the investigated metallohelices alone or the DNA condensates induced by the metallohelices and their transfection efficiency. Thus, it is reasonable to conclude that cytotoxicity of the investigated metallohelices was not a crucial factor that would essentially reduce their potential to act as gene delivery vectors.

Transfection studies

To explore the potential of metallohelices as gene delivery vectors, gene transfection was tested on HEK 293 cells by using the green fluorescent protein (GFP) reporter gene. Fluorescent microscopy images in Figure 6 showed that cells expressing GFP provided green fluorescence following excitation at 488 nm. Green fluorescent spots of various intensities correspond to cells producing various levels of GFP. The image of control cells incubated with DNA in the absence of a metallohelix shows no fluorescence (Figure 6A). It can be observed that cells treated with DNA condensates of **1** were rarely GFP positive, with the Λ-enantiomer being slightly more effective than the Δ-enantiomer. Significantly more cells were GFP positive following incubation with DNA condensates of **2** and **3** (Figure 6D–G). The most efficient transfection was mediated by DNA condensates formed in the presence of **Λ-2** (Figure 6D).

The transfection efficiency of metallohelices was further quantified by flow cytometry. The results in Figure 7 confirm low transfection activity for **Λ-1** and **Δ-1** as their DNA condensates induced GFP fluorescence only in a limited number of cells. Nevertheless, the bar graph in Figure 7B shows that **Λ-1** was slightly more potent than **Δ-1**. DNA condensates formed in the presence of **2** and **3** were apparently much more successful in entering the cells and delivering the cargo. The plasmid DNA was released from the metallohelices–DNA complexes, and substantial amounts of GFP were produced inside cells. The Λ-enantiomers of **2** and **3** were more potent than the Δ-enantiomers. Consis-

tently with the previous results, the highest gene transfection efficiency was observed for **Λ-2**.

CONCLUSIONS

In summary, the results showed that Fe(II) metallohelices are potent DNA condensing agents capable of mediating gene transfection. Metallohelices **2** and **3** were demonstrated to promote the formation of cationic DNA nanoparticles that were successfully taken up and processed by cells. The size of DNA condensates formed with **2** and **3** falls within the range of ∼30–200 nm that is favorable for cellular uptake, and the high positive surface charge (30–40 mV) of DNA condensates ensures both good stability and enhanced internalization by cells.

On the other hand, the transfection activity of the shorter and more compact metallohelix **1** was much lower. The mechanistic studies revealed that the binding of **1** to ds DNA depends mostly on the electrostatic interactions that are strongly affected by the ionic strength. As a result, DNA binding of **1** is weakened, and DNA condensates promoted by **1** are rapidly unfolded in the presence of endogenous cations such as Na^+, K^+ or Mg^{2+}. The poor stability of DNA condensates of **1** and their propensity for aggregation are probably responsible for their low cellular uptake. Conversely, the DNA condensates of **2** and **3** are much more stable and resistant towards decondensation by Na^+, K^+ or Mg^{2+} than those formed by **1**. The higher transfection efficiency of **2** compared to **3** is consistent with the higher cellular uptake of DNA condensates formed by **2,** which can be associated with the elevated surface charge that facilitates permeability through the negatively charged cell membrane. It is worth noting that the Λ-enantiomers of **2** and **3**, despite being slightly more cytotoxic, exhibited higher transfection efficiency than the Δ-enantiomers.

Overall, this study shows for the first time that metallohelical assemblies can be used as nonviral gene delivery vectors. The modular structure and our ability to modify architecture and functionality will allow us to study structure activity relationships, leading to mechanistic information and design of systems with further enhanced and perhaps targetable DNA transfection properties.

DATA AVAILABILITY

All data that support the findings of this study are available on request from the corresponding author, VB.

SUPPLEMENTARY DATA

Supplementary Data are available at NAR Online.

FUNDING

Czech Science Foundation [20-00735S]. Funding for open access charge: Czech Academy of Sciences, Institute of Biophysics.
Conflict of interest statement. None declared.

REFERENCES

1. Dunbar,C.E., High,K.A., Joung,J.K., Kohn,D.B., Ozawa,K. and Sadelain,M. (2018) Gene therapy comes of age. *Science*, **359**, eaan4672.
2. Mulligan,R.C. (1993) The basic science of gene therapy. *Science*, **260**, 926–932.
3. Yang,Y., Nunes,F.A., Berencsi,K., Gönczöl,E., Engelhardt,J.F. and Wilson,J.M. (1994) Inactivation of E2a in recombinant adenoviruses improves the prospect for gene therapy in cystic fibrosis. *Nat. Genet.*, **7**, 362–369.
4. Ledford,H. (2015) Gene therapy sees early success against progressive blindness: treatments for inherited eye diseases show promise in clinical trials, but worries linger over how long the beneficial effects will last. *Nature*, **526**, 487–489.
5. Pahle,J. and Walther,W. (2016) Vectors and strategies for nonviral cancer gene therapy. *Exp. Opin. Biol. Ther.*, **16**, 443–461.
6. Ibraheem,D., Elaissari,A. and Fessi,H. (2014) Gene therapy and DNA delivery systems. *Int. J. Pharm.*, **459**, 70–83.
7. Mintzer,M.A. and Simanek,E.E. (2009) Nonviral vectors for gene delivery. *Chem. Rev.*, **109**, 259–302.
8. Thomas,T.J., Tajmir-Riahi,H.A. and Thomas,T. (2016) Polyamine-DNA interactions and development of gene delivery vehicles. *Amino Acids*, **48**, 2423–2431.
9. Soliman,M., Allen,S., Davies,M.C. and Alexander,C. (2010) Responsive polyelectrolyte complexes for triggered release of nucleic acid therapeutics. *Chem. Commun.*, **46**, 5421–5433.
10. Green,J.J., Langer,R. and Anderson,D.G. (2008) A combinatorial polymer library approach yields insight into nonviral gene delivery. *Acc. Chem. Res.*, **41**, 749–759.
11. Gabrielson,N.P., Lu,H., Yin,L., Li,D., Wang,F. and Cheng,J. (2012) Reactive and bioactive cationic α-helical polypeptide template for nonviral gene delivery. *Angew. Chem. Int. Ed.*, **51**, 1143–1147.
12. Zhi,D., Zhang,S., Cui,S., Zhao,Y., Wang,Y. and Zhao,D. (2013) The headgroup evolution of cationic lipids for gene delivery. *Bioconjug. Chem.*, **24**, 487–519.
13. Lai,W.-F. (2014) Cyclodextrins in non-viral gene delivery. *Biomaterials*, **35**, 401–411.
14. Yang,J., Zhang,Q., Chang,H. and Cheng,Y. (2015) Surface-engineered dendrimers in gene delivery. *Chem. Rev.*, **115**, 5274–5300.
15. Kotterman,M.A., Chalberg,T.W. and Schaffer,D.V. (2015) Viral vectors for gene therapy: translational and clinical outlook. *Annu. Rev. Biomed. Eng.*, **17**, 63–89.
16. Thomas,C.E., Ehrhardt,A. and Kay,M.A. (2003) Progress and problems with the use of viral vectors for gene therapy. *Nat. Rev. Genet.*, **4**, 346–358.
17. Yin,H., Kanasty,R.L., Eltoukhy,A.A., Vegas,A.J., Dorkin,J.R. and Anderson,D.G. (2014) Non-viral vectors for gene-based therapy. *Nat. Rev. Genet.*, **15**, 541–555.
18. Li,G.-Y., Guan,R.-L., Ji,L.-N. and Chao,H. (2014) DNA condensation induced by metal complexes. *Coord. Chem. Rev.*, **281**, 100–113.
19. Bhat,S.S., Kumbhar,A.S., Kumbhar,A.A., Khan,A., Lönnecke,P. and Hey-Hawkins,E. (2011) Ruthenium(II) polypyridyl complexes as carriers for DNA delivery. *Chem. Commun.*, **47**, 11068–11070.
20. Bhat,S.S., Kumbhar,A.S., Kumbhar,A.A. and Khan,A. (2012) Efficient DNA condensation induced by ruthenium(II) complexes of a bipyridine-functionalized molecular clip ligand. *Chem. Eur. J.*, **18**, 16383–16392.
21. Yu,B., Chen,Y., Ouyang,C., Huang,H., Ji,L. and Chao,H. (2013) A luminescent tetranuclear ruthenium(II) complex as a tracking non-viral gene vector. *Chem. Commun.*, **49**, 810–812.
22. Bhat,S.S., Revankar,V.K., Khan,A., Pinjari,R.V. and Necas,M. (2017) Luminescent ruthenium(II) polypyridyl complexes as nonviral carriers for DNA delivery. *Chem. Asian J.*, **12**, 254–264.
23. Yu,B., Ouyang,C., Qiu,K., Zhao,J., Ji,L. and Chao,H. (2015) Lipophilic tetranuclear ruthenium(II) complexes as two-photon luminescent tracking non-viral gene vectors. *Chem. Eur. J.*, **21**, 3691–3700.
24. Rouwei,J., Jun,Y., Si,H., Xianggao,M. and Changlin,L. (2013) Cobalt(II)-polybenzimidazole complexes as a nonviral gene carrier: effects of charges and benzimidazolyl groups. *Curr. Drug Deliv.*, **10**, 122–133.

25. Liu,L., Zhang,H., Meng,X., Yin,J., Li,D. and Liu,C. (2010) Dinuclear metal(II) complexes of polybenzimidazole ligands as carriers for DNA delivery. *Biomaterials*, **31**, 1380–1391.
26. Huang,X., Dong,X., Li,X., Meng,X., Zhang,D. and Liu,C. (2013) Metal–polybenzimidazole complexes as a nonviral gene carrier: effects of the DNA affinity on gene delivery. *J. Inorg. Biochem.*, **129**, 102–111.
27. Yin,J., Meng,X., Zhang,S., Zhang,D., Wang,L. and Liu,C. (2012) The effect of a nuclear localization sequence on transfection efficacy of genes delivered by cobalt(II)–polybenzimidazole complexes. *Biomaterials*, **33**, 7884–7894.
28. Liu,L., Zhang,H., Meng,X., Yin,J., Li,D. and Liu,C. (2010) Dinuclear metal(II) complexes of polybenzimidazole ligands as carriers for DNA delivery. *Biomaterials*, **31**, 1380–1391.
29. Bao,F.-F., Xu,X.-X., Zhou,W., Pang,C.-Y., Li,Z. and Gu,Z.-G. (2014) Enantioselective DNA condensation induced by heptameric lanthanum helical supramolecular enantiomers. *J. Inorg. Biochem.*, **138**, 73–80.
30. Zhang,D., Wang,J. and Xu,D. (2016) Cell-penetrating peptides as noninvasive transmembrane vectors for the development of novel multifunctional drug-delivery systems. *J. Control Release*, **229**, 130–139.
31. Malina,J., Hannon,M.J. and Brabec,V. (2015) Iron(II) supramolecular helicates condense plasmid DNA and inhibit vital DNA-related enzymatic activities. *Chem. Eur. J.*, **21**, 11189–11195.
32. Crlikova,H., Malina,J., Novohradsky,V., Kostrhunova,H., Vasdev,R.A.S., Crowley,J.D., Kasparkova,J. and Brabec,V. (2020) Antiproliferative activity and associated DNA interactions of [Co2L3]6+ cylinders derived from bis(bidentate) 2-pyridyl-1,2,3-triazole ligands. *Organometallics*, **39**, 1448–1455.
33. Hrabina,O., Malina,J., Kostrhunova,H., Novohradsky,V., Pracharova,J., Rogers,N., Simpson,D.H., Scott,P. and Brabec,V. (2020) Optically pure metallohelices that accumulate in cell nuclei, condense/aggregate DNA, and inhibit activities of DNA processing enzymes. *Inorg. Chem.*, **59**, 3304−3311.
34. Howson,S.E., Bolhuis,A., Brabec,V., Clarkson,G.J., Malina,J., Rodger,A. and Scott,P. (2012) Optically pure, water-stable metallo-helical 'flexicate' assemblies with antibiotic activity. *Nature Chem.*, **4**, 31–36.
35. Faulkner,A.D., Kaner,R.A., AbdallahQasem,M.A., Clarkson,G., Fox,D.J., Gurnani,P., Howson,S.E., Phillips,R.M., Roper,D.I., Simpson,D.H. *et al.* (2014) Asymmetric triplex metallohelices with high and selective activity against cancer cells. *Nat. Chem.*, **6**, 797–803.
36. Kaner,R.A., Allison,S.J., Faulkner,A.D., Phillips,R.M., Roper,D.I., Shepherd,S.L., Simpson,D.H., Waterfield,N.R. and Scott,P. (2016) Anticancer metallohelices: nanomolar potency and high selectivity. *Chem. Sci.*, **7**, 951–958.
37. Simpson,D.H., Hapeshi,A., Rogers,N.J., Brabec,V., Clarkson,G.J., Fox,D.J., Hrabina,O., Kay,G.L., King,A.K., Malina,J. *et al.* (2019) Metallohelices that kill Gram-negative pathogens using intracellular antimicrobial peptide pathways. *Chem. Sci.*, **10**, 9708–9720.
38. Song,H., Rogers,N.J., Brabec,V., Clarkson,G.J., Coverdale,J.P.C., Kostrhunova,H., Phillips,R.M., Postings,M., Shepherd,S.L. and Scott,P. (2020) Triazole-based, optically-pure metallosupramolecules; highly potent and selective anticancer compounds. *Chem. Commun.*, **56**, 6392–6395.
39. Wilson,R.W. and Bloomfield,V.A. (1979) Counterion-induced condensation of deoxyribonucleic acid. A light-scattering study. *Biochemistry*, **18**, 2192–2196.
40. Hibino,K., Yoshikawa,Y., Murata,S., Saito,T., Zinchenko,A.A. and Yoshikawa,K. (2006) Na+ more strongly inhibits DNA compaction by spermidine (3+) than k+. *Chem. Phys. Lett.*, **426**, 405–409.
41. Pratihar,S., Suseela,Y.V. and Govindaraju,T. (2020) Threading intercalator-induced nanocondensates and role of endogenous metal ions in decondensation for DNA delivery. *ACS Appl. Bio Mater.*, **3**, 6979–6991.
42. Malina,J., Kostrhunova,H., Scott,P. and Brabec,V. (2021) FeII metallohelices stabilize DNA G-quadruplexes and downregulate the expression of G-quadruplex-regulated oncogenes. *Chem. Eur. J.*, **27**, 11682–11692.
43. Hansma,H.G., Golan,R., Hsieh,W., Lollo,C.P., Mullen-Ley,P. and Kwoh,D. (1998) DNA condensation for gene therapy as monitored by atomic force microscopy. *Nucleic Acids Res.*, **26**, 2481–2487.
44. Pjura,P.E., Grzeskowiak,K. and Dickerson,R.E. (1987) Binding of hoechst 33258 to the minor groove of B-DNA. *J. Mol. Biol.*, **197**, 257–271.
45. Burres,N.S., Frigo,A., Rasmussen,R.R. and McAlpine,J.B. (1992) A colorimetric microassay for the detection of agents that interact with DNA. *J. Nat. Prod.*, **55**, 1582–1587.
46. Riddick,T.M. (1968) In: *Control of colloid stability through zeta potential : with a closing chapter on its relationship to cardiovascular disease*. Published for Zeta-Meter, Inc., by Livingston Pub. Co., Wynnewood, Pa, Vol. **1**.